Saturn chorus intensity variations

J. D. Menietti,[1] P. Schippers,[2] Y. Katoh,[3] J. S. Leisner,[4] G. B. Hospodarsky,[1]
D. A. Gurnett,[1] and O. Santolik[5,6]

Received 13 May 2013; revised 30 July 2013; accepted 22 August 2013; published 11 September 2013.

[1] Whistler mode chorus plasma wave emissions have been observed at Saturn near the magnetic equator and the source region. During crossings of the magnetic equator along nearly constant L shells, the Cassini Radio and Plasma Wave Science Investigation often observes a local decrease in whistler mode intensity and bandwidth closest to the magnetic equator, where linear growth appears to dominate, with nonlinear structures appearing at higher latitudes and higher frequencies. We investigate linear growth rate using the Waves in a Homogeneous, Anisotropic, Multi-component Plasma dispersion solver and locally observed electron phase space density measurements from the Electron Spectrometer sensor of the Cassini Plasma Spectrometer Investigation to determine the parameters responsible for the variation in chorus intensity and bandwidth. We find that a temperature anisotropy ($T_\perp/T_\parallel \sim 1.3$) can account for linear spatiotemporal growth rate of whistler mode waves, which provides a majority of the observed frequency-integrated power. At the highest frequencies, intense, nonlinear, frequency-drifting structures (drift rates ~ 200 Hz/s) are observed a few degrees away from the equator and can account for a significant fraction of the total power. Chorus emission at higher frequencies is distinct from lower frequency whistler mode emission and is sometimes correlated with simultaneously observed low-frequency electromagnetic ion cyclotron waves. These electromagnetic ion cyclotron waves appear to modulate a slow frequency drift (~15 Hz/s) which develops into nonlinear growth with much larger frequency drift associated only with the higher-frequency chorus.

Citation: Menietti, J. D., P. Schippers, Y. Katoh, J. S. Leisner, G. B. Hospodarsky, D. A. Gurnett, and O. Santolik (2013), Saturn chorus intensity variations, *J. Geophys. Res. Space Physics*, *118*, 5592–5602, doi:10.1002/jgra.50529.

1. Introduction

[2] Chorus emission at the outer planets has been recently reviewed by *Hospodarsky et al*. [2012] and *Menietti et al.* [2012], who compare and contrast the wave amplitudes and source location at Earth, Jupiter, and Saturn. Chorus emissions at Earth are known to have source regions near the magnetic equator and to be a significant source of electron acceleration in the Van Allen radiation belts. Recent studies at Jupiter [*Horne et al.*, 2008] have shown that similar processes may be acting there to accelerate electrons. *Sphrits et al*. [2012] have conducted a comparison of stochastic electron acceleration at Earth, Jupiter, and Saturn and have found that while chorus emission at Earth and Jupiter appears to be an effective source of pitch angle scattering and consequent stochastic electron acceleration, intense dust clouds at Saturn may inhibit the efficiency of the process, as earlier suggested in the work of *Mauk and Fox* [2010]. However, *Summers et al*. [2012] have more recently shown that by including relativistic effects in the equations, whistler mode emissions seem to play a significant role in nonlinear wave-particle interactions at Saturn.

[3] There are two general types of whistler mode emission present in planetary magnetospheres, hiss, and chorus. Whistler mode emission exists at frequencies less than either the plasma frequency, f_p, or the cyclotron frequency, f_c, whichever is lower, but close to the magnetic equator in the inner magnetospheric region $f_p > f_c$. Hiss has a featureless spectrum and is typically at lower frequencies than chorus, which often has a banded structure and, at high resolution, displays a fine structure of many frequency-drifting tones or chirps that have larger than typical spectral densities. These structures are the result of the nonlinear nature of chorus and resonant wave trapping of electrons as described, for instance, by *Nunn et al*. [1997], *Trakhtengerts et al*. [1996], *Trakhtengerts* [1999], *Omura and Summers* [2004, 2006], and *Katoh and Omura* [2004, 2006a, 2006b, 2007a, 2007b, 2011]. *Omura et al*. [2007] have extended the work of *Omura and Summers* [2006] to describe an extremely efficient nonlinear mechanism for accelerating high-energy electrons (seed electrons of approximately several hundred

[1]Department of Physics and Astronomy, University of Iowa, Iowa City, Iowa, USA.
[2]LESIA, Observatoire de Paris, Meudon Cedex, France.
[3]Department of Geophysics, Graduate School of Science, Tohoku University, Sendai, Japan.
[4]Physics and Astronomy, University of Leicester, Leicester, UK.
[5]Institute of Atmospheric Physics, Prague, Czech Republic.
[6]Faculty of Mathematics and Physics, Charles University, Prague, Czech Republic.

Corresponding author: J. D. Menietti, Department of Physics and Astronomy, University of Iowa, 210 Van Allen Hall, Iowa City, IA 52242-1479, USA. (john-menietti@uiowa.edu)

2169-9380/13/10.1002/jgra.50529

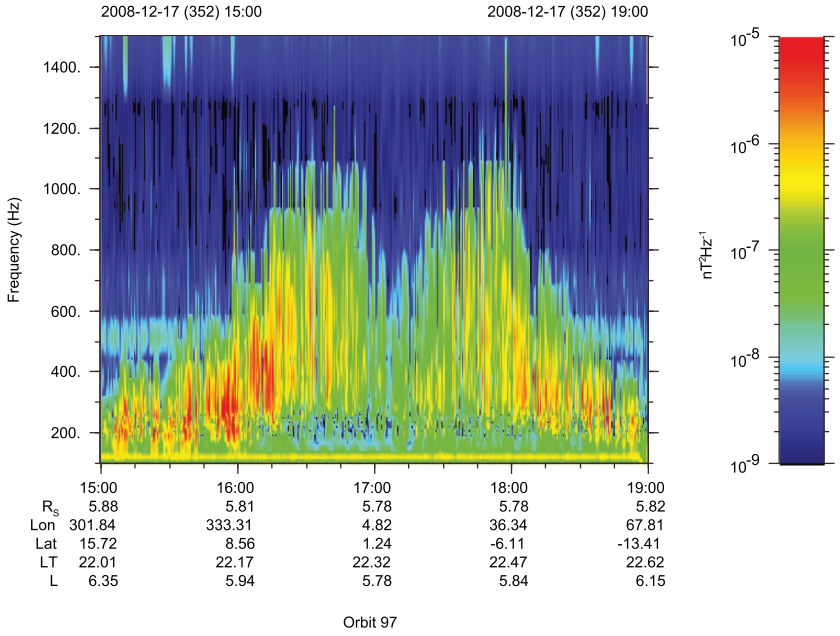

Figure 1. A frequency time spectrogram with magnetic field spectral density color coded. The chorus data are from the low-rate receiver of the RPWS during an equator crossing at near-constant L shell. Note the decrease in chorus bandwidth and intensity near the magnetic equator crossing (~17:00 to ~17:20).

keV) to a few MeV in only a few seconds. This process is called relativistic turning acceleration by the authors and requires relatively large amplitude chorus emissions and an initial population of mildly energetic electrons. In addition, *Summers and Omura* [2007] describe an ultrarelativistic acceleration mechanism for electrons that is possible at the outer planets. *Bortnik et al*. [2008] have performed test-particle modeling for oblique waves as well, finding that nonlinear phase-trapping leads to rapid, large increase in energy and pitch angle for a small portion of test particles.

[4] *Santolik et al*. [2009] may have been the first to report that terrestrial chorus emission intensity actually increased with latitude from the magnetic equator. *Haque et al*. [2012] reported that terrestrial chorus intensities measured by the Cluster spacecraft generally increased exponentially away from the magnetic equator according to a constant spatial growth factor. *Menietti et al*. [2012, 2013] reported a similar decrease of chorus intensity and bandwidth near the magnetic equator for Saturn chorus emissions. *Summers et al*. [2012] were the first to analyze the nonlinear evolution and saturation of whistler mode waves away from the magnetic equator. They report convective growth due to nonlinear wave trapping and a saturation process partly due to a combination of adiabatic effects and a decreasing resonant current with latitude.

[5] In the present study we examine examples of chorus intensity near the source region and relate it to in situ electron phase space density (PSD) measurements. We note that nonlinear chorus emission at Saturn appears only after linear growth near the magnetic equator. We also report on interesting modulation of chorus power that may be due to low-frequency electromagnetic ion cyclotron waves.

2. Observations and Analysis

[6] Figure 1 is an example of chorus emission observed by the Cassini Radio and Plasma Wave Science instrument (RPWS) [*Gurnett et al*., 2004] magnetic field search coils on board Cassini during a high-inclination orbit when the spacecraft crossed the equator from north to south at near-constant L shell. This plot shows rather intense chorus and

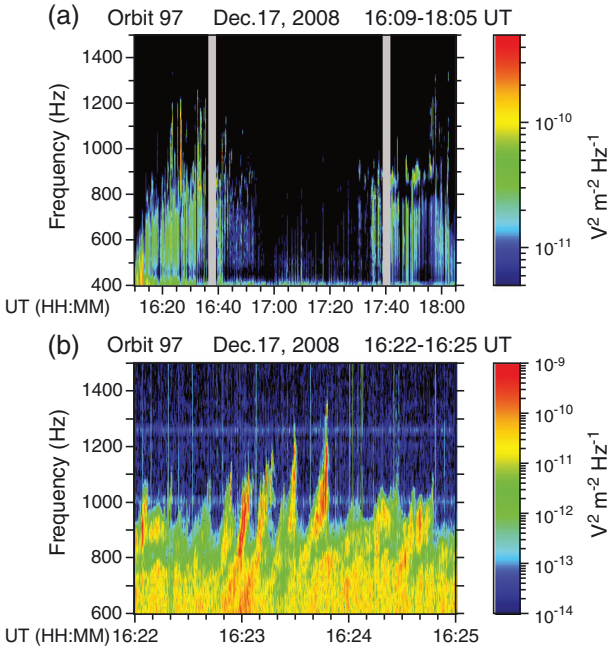

Figure 2. (a, b) A higher-resolution spectrogram of the electric field spectral density obtained by the wideband receiver (WBR) for the same pass as Figure 1. Discrete nonlinear chorus features which extend to higher frequencies are seen a few degrees away from the magnetic equator. Some of these are seen at higher resolution in Figure 2b.

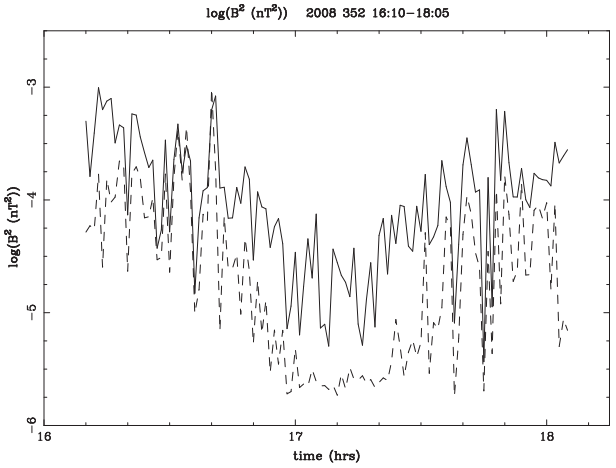

Figure 3. Frequency-integrated power for the time interval 16:10 to 18:05. Most power is contained in the lower frequency emissions (solid line), but there are periods when the higher-frequency nonlinear chorus power (dashed line) is comparable to and even exceeds the lower frequency emissions.

whistler mode emission at frequencies less than the cyclotron frequency (which covers the range $2500 < f_c < 2800$ Hz over the time period). Within about 1.5° of the magnetic equator (16:57 to 17:21), the whistler mode emission intensity and bandwidth decrease with the lowest intensity observed closest to the magnetic equator near 17:10. In Figure 2a, we show a higher-resolution plot obtained by the Cassini RPWS Wideband Receiver (WBR), which measures electric field intensity on one of the three available antennas. Nonlinear, frequency-drifting features are seen at the highest frequencies of the chorus ($\gtrsim$ 800 Hz). In Figure 2b, we show a higher-resolution portion of Figure 2a delineating some of the nonlinear drifting frequency features. The frequency dispersion of the waves is seen as broad banded fine structures. These features are absent nearest the magnetic equator and extend to higher frequency and larger bandwidth with increasing latitude, peaking in power near ±5°–6°, before they fall off. The broadband spikes nearest the magnetic equator in Figure 2a are electrostatic bursts, possibly related to electron beams.

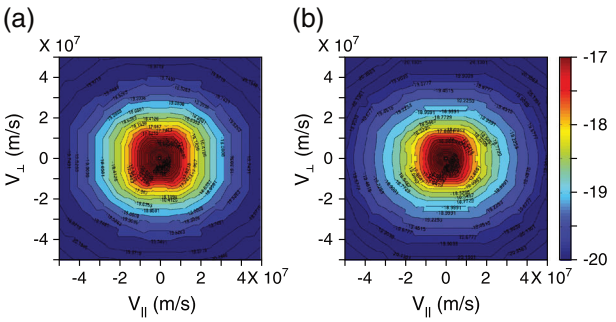

Figure 4. Contours of the electron phase space distribution for a 2 s time period when the spacecraft was (a) near the magnetic equator at 17:11:10 and (b) away from the equator at 16:23:13 during a time period when we observe nonlinear drifting frequencies.

Table 1. Plasma Parameters Near 16:23:13

Plasma Component	$n_e(m^{-3})$	$V_{t\|\|}$ (m/s)	$T_\perp/T_\|\|$
Cold	3.76×10^6	1.73×10^6	1.17
Warm1	2.44×10^5	5.52×10^6	0.83
Warm2	5.15×10^4	1.86×10^7	1.42
Core electrons	1.83×10^7	1.33×10^5	1.0
Core ions	2.24×10^7	3.10×10^3	1.0

[7] We have calculated the frequency-integrated power (proportional to B^2) of whistler mode emissions over the lower frequencies which are dominated by relatively weak emissions displaying no frequency-drifting signatures and separately over higher frequencies where more intense, frequency-drifting features occur. In Figure 3, we plot the results for the time interval 16:10 to 18:05 for which high-resolution electric field WBR measurements exist. Most power is contained in the lower frequency (typically $\lesssim$ 600 Hz) emissions (solid line), but there are periods when the higher frequency nonlinear chorus power is comparable to and even exceeds the lower frequency emissions.

[8] For specific times, we have investigated the electron phase space distribution (PSD) obtained from the electron spectrometer (ELS) which is one of three sensors of the Cassini Plasma Spectrometer (CAPS) instrument on board the Cassini spacecraft [*Young et al.*, 2004]. In Figure 4, we display contours of the PSD obtained for a 2 s time period when the spacecraft was near the magnetic equator and for which we have a sufficient pitch angle distribution at 17:11:10 and also away from the equator at 16:23:13 during a time period when we observe nonlinear drifting frequencies. For each of these observed distributions, we have performed a nonlinear least squares fit to a bi-Maxwellian. Using the Waves in a Homogeneous, Anisotropic, Multi-component Plasma (WHAMP) dispersion solver [*Rönnmark*, 1982, 1983], we have calculated the real and imaginary frequencies, f, f_i (linear temporal growth rate) versus wave number, **k**, for these electron distributions. The modeling parameters for the plasma components are listed in Tables 1 and 2, where n_e is the electron number density and $V_{t\|\|}$ is the parallel thermal velocity.

[9] In Figures 5a and 5b, we overplot the observed and fitted electron distributions, and in Figures 5c and 5d, we display f and f_i versus wave number, **k**, for the model distributions. Both plots show modest linear temporal growth of whistler mode waves over a range ~50 Hz < f < 450 Hz near the equator (17:11) and ~100 Hz < f < 800 Hz near 5° latitude (16:23) where nonlinear emission is also observed. The weaker "hiss-like" emission near the equator is observed to extend to perhaps 600 Hz, somewhat higher than calculated. Both of the plots indicate growth rates reaching approximately $f_i/f_c \sim 10^{-4}$, but linear growth extends to higher frequency for the distribution near 16:23:13. The frequency extent of the observed nonlinear signatures near 16:23 is approximately 800 Hz < f < 1200 Hz. As shown by simulation results of the chorus generation [cf. *Katoh and Omura*, 2007a], the frequency range of the generated chorus is significantly different from that estimated by the linear theory and can extend to higher frequency range. The calculated wave normal angle is near zero for each time period as determined from the dispersion solver and growth rate calculations.

[10] We have also evaluated the spatial growth, $\gamma_s = \omega_i/v_g$ (v_g = group velocity) for the whistler mode emissions

Table 2. Plasma Parameters Near 17:10:11

Plasma Component	$n_e(m^{-3})$	$V_{t\|\|}$ (m/s)	$T_\perp/T_\|\|$
Cold	1.30×10^7	2.1×10^6	1.19
Warm1	1.90×10^5	9.44×10^6	1.08
Warm2	2.54×10^4	3.60×10^7	1.33
Core electrons	2.69×10^7	1.33×10^5	1.0
Core ions	4.01×10^7	3.10×10^3	1.0

observed near the equator (Table 2 parameters), and plotted the results versus f in Figure 6. The γ_s decreases by about an order of magnitude over the frequency range ~125Hz < f < ~450Hz with a peak near 125 Hz. In Figure 7, we plot the calculated spatial growth overlaid with the observed frequency-integrated power for all emission frequencies. The frequency-integrated power is evaluated over the range 200 Hz < f < 1500 Hz. The minimum frequency is set by interference observed for f < 200 Hz, and the maximum frequency is chosen to be above all observed chorus emission. A least squares fit to the peaks of the integrated power is shown (dashed lines). We have used the calculated spatial growth as a function of frequency to determine the expected frequency-integrated power as a function of time (latitude). This was done using the observed power levels near the magnetic equator and assuming that the spatial growth remains constant in time and space along the field line in the direction away from the equator into each hemisphere. This is plotted as a dash-dotted curve in Figure 7 and is significantly larger than the observed integrated power levels. This indicates that spatial growth near the equator is more than sufficient to provide the observed power as a function of latitude, but γ_s is not constant during the propagation time. For 200 Hz < f < 450 Hz, $v_g \approx 5\times10^6$ m/s. To propagate 5° in latitude would require ~6 s.

2.1. Effects of Ion Cyclotron Waves

[11] In Figure 8, we display a 10 min interval of wideband data with an expanded frequency range that includes chorus emissions (f < f_c) and electrostatic cyclotron harmonic (ECH) emissions (f > f_c). The ECH emissions show a periodicity of about 14 s, obtained by Fourier analysis, that is not due to the spacecraft rotation (Cassini has a fixed attitude at this time). Figure 9a is a higher-resolution version of Figure 8 where it appears the chorus and ECH emission have nearly the same period. The drifting frequency chorus emissions at higher frequencies have a distinct morphology. There is a slowly frequency-drifting part with a drift rate of ~ 10–20 Hz/s and a distinct intense fine structure component with a higher drift rate which is consistent with the theory of *Omura et al*. [2008]. The fine structure of the frequency-drifting signatures with drift rates ~ 200 Hz/s is shown in Figure 9a as an inset [cf. *Menietti et al*., 2013]. In Figures 9a and 9b, we see that the drifting frequency chorus emissions are most intense near and within the period of time when the ECH emissions are least intense. In Figure 9c, a 2 min interval a few minutes later, the drifting frequency chorus emissions

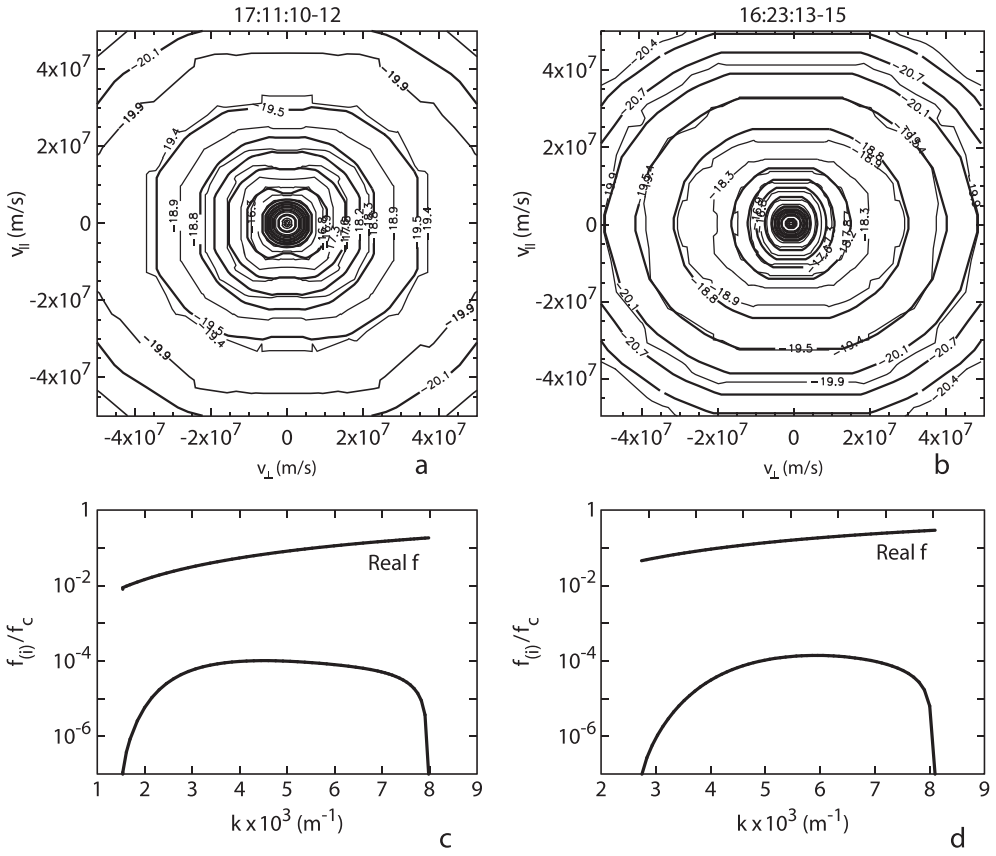

Figure 5. Overplots of the observed and model (bold) electron PSD (a) near the magnetic equator and (b) near 16:23:13. (c, d) Real f and f_i versus wave number, **k**, calculated for the distributions of Figures 5a and 5b, respectively.

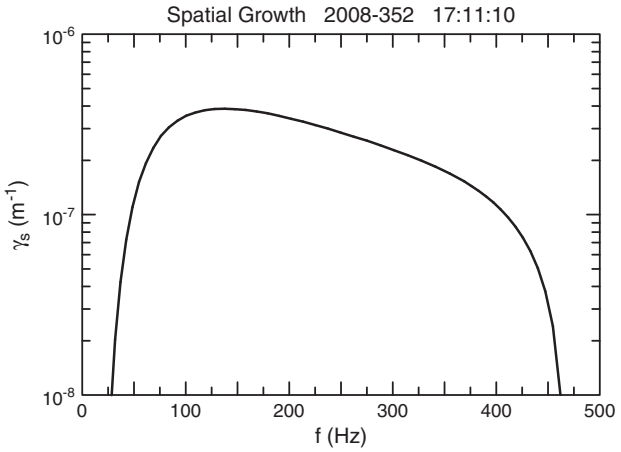

Figure 6. Spatial growth, $\gamma_s = \omega_i/v_g$, versus f for the whistler mode emissions observed near the equator (17:11). The γ_s decreases by a factor of about 3 in the approximate frequency range 100Hz < f < 400Hz with a peak near 125 Hz.

are seen to vary in phase relative to the ECH emission. The periodicity of the ECH and probably the chorus emissions as well is due to the presence of very low frequency, moderate intensity electromagnetic ion cyclotron waves (EMICs) that are also observed near the magnetic equator at these radial distances [cf. *Leisner et al*., 2006; *Russell et al*., 2006]. These waves have a source region near the magnetic equator, where they are actually less intense, and propagate away from it as reported by *Leisner et al*. [2011]. The ability of ion cyclotron waves to heat ions and electrons has been shown in the past at Earth [cf. *Lysak et al*., 1980; *Carlson et al*., 1998] and at Saturn [*Menietti et al*., 2011]. In Figures 10a and 10b, we show plots of the magnetic field oscillations obtained by the Cassini magnetometer [*Dougherty et al*., 2005] during times that overlap the RPWS data shown in Figure 9. The 4 Hz magnetometer data were analyzed with a 512 point running fast Fourier transform, with a 50% overlap between windows. In Figure 10a, we show the average power spectrum between 16:19 and 16:25. The dark line labeled "Trans." is the transverse wave power (perpendicular to the magnetic field). The lighter line labeled "Comp." is the compressional wave power (along the magnetic field). The vertical line near 0.1 Hz is the O^+ gyrofrequency during this period of time. Figure 10b is a spectrogram of the total ion cyclotron wave power during this equatorial crossing (~17:10). The black line marks the O^+ gyrofrequency across the interval. The difference between the peak wave frequency and the gyrofrequency in the two hemispheres is due to Doppler shift [*Leisner et al*., 2011]. The EMIC waves are due to water group W^+ (H_3O^+, H_2O^+, HO^+, O^+) and to O_2^+ ions [cf. *Leisner et al*., 2006; *Russell et al*., 2006]. Thus, the observed wave periods are variable and appear to be in the range of 12 to 15 s.

[12] Although not constant, the period of the EMIC waves is frequently the same as the modulation of power of the ECH and chorus emissions shown in Figure 9. The low-frequency ($f \sim 7 \times 10^{-2}$ Hz) EMIC waves have $\Delta B \sim 2$nT and modulate the amplitude of the much higher frequency ECH emissions seen overplotted (in normalized, arbitrary units) in Figure 10c. The power of the EMIC waves is orders of magnitude larger than the ECH and chorus emissions. In Figure 10d, we overplot the amplitude of the ion cyclotron waves with the chorus amplitude (in normalized, arbitrary units) averaged over the frequency range 500 Hz < f < 1500 Hz. Unlike the ECH waves, the chorus amplitudes are not well correlated with the EMIC waves; however, there are times when the peak chorus amplitudes at the highest frequencies coincide with peaks in the EMIC wave amplitudes. We note that the ECH waves are electrostatic and are therefore generated locally, whereas the source region of the chorus and whistler mode emission is likely not local. It is therefore not surprising to note a poorer correlation between the EMIC waves and the whistler mode emission.

[13] *Beesho and Menietti* [2007] have shown how EMIC waves stimulate the growth of terrestrial auroral kilometric radiation (AKR). The latter authors performed particle-in-cell simulations of AKR in the presence of EMIC waves, showing that the AKR growth is stimulated in phase with the energy density of the EMIC electric field. It is conceivable that a similar process is taking place here with the EMIC waves stimulating the growth of ECH and possibly chorus emission as well. *Chaston et al*. [2002] have studied EMIC waves generated in the terrestrial auroral region by inverse Landau interaction with upward electron beams with E > 100 eV. Oscillations of the electron count rate, obtained at high resolution, are seen at the period of the EMIC waves in their Figure 1. More recently, *Li et al*. [2011] using terrestrial Time History of Events and Macroscale Interactions during Substorms (THEMIS) spacecraft data have shown that compressional Pc4-5 pulsations modulate the integrated chorus amplitudes. These authors then determined that linear growth rates were more effectively modulated by changes in the ratio of resonant electrons to the total electrons compared to changes in the electron temperature anisotropy.

2.2. Electron Differential Energy Flux

[14] In Figure 11, we display plots of differential energy flux (DEF) obtained by the Cassini CAPS/ELS instrument for 2008 day 352 from 16:20 to 16:30. Shown are plots for three of the eight fan-arranged anodes of the instrument, with the bottom panel showing the pitch angle coverage for each

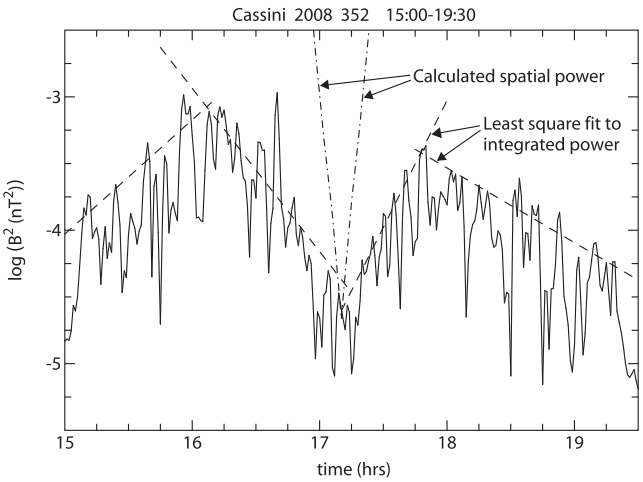

Figure 7. Calculated spatial growth as a function of latitude (time) overlaid with the observed frequency-integrated power for all emission frequencies.

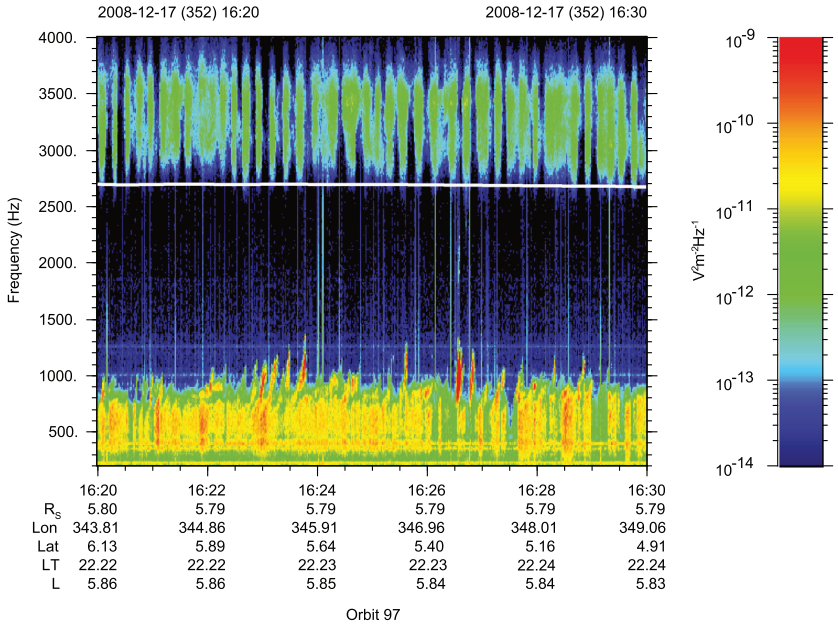

Figure 8. A 10 min interval spectrogram of wideband high-resolution electric field spectral density. The frequency range is expanded to include chorus emissions ($f < f_c$, shown by the white line) and electrostatic cyclotron harmonic (ECH) emissions ($f > f_c$). The ECH emissions show a periodicity of about 14 s that is not due to the spacecraft rotation.

anode as a function of time. The pitch angle coverage changes due to the motion of an actuator [cf. *Young et al.*, 2004]. In these plots, we see two distinct electron populations for $E > 100$eV: a higher energy (1keV) more pancake distribution which we previously displayed in Figure 5 and fit to $T_\perp/T_\parallel > 1$ (the "Warm2" component in Tables 1 and 2), and an interesting lower energy population (between 100eV and 1keV) which shows a dependence on pitch angle,

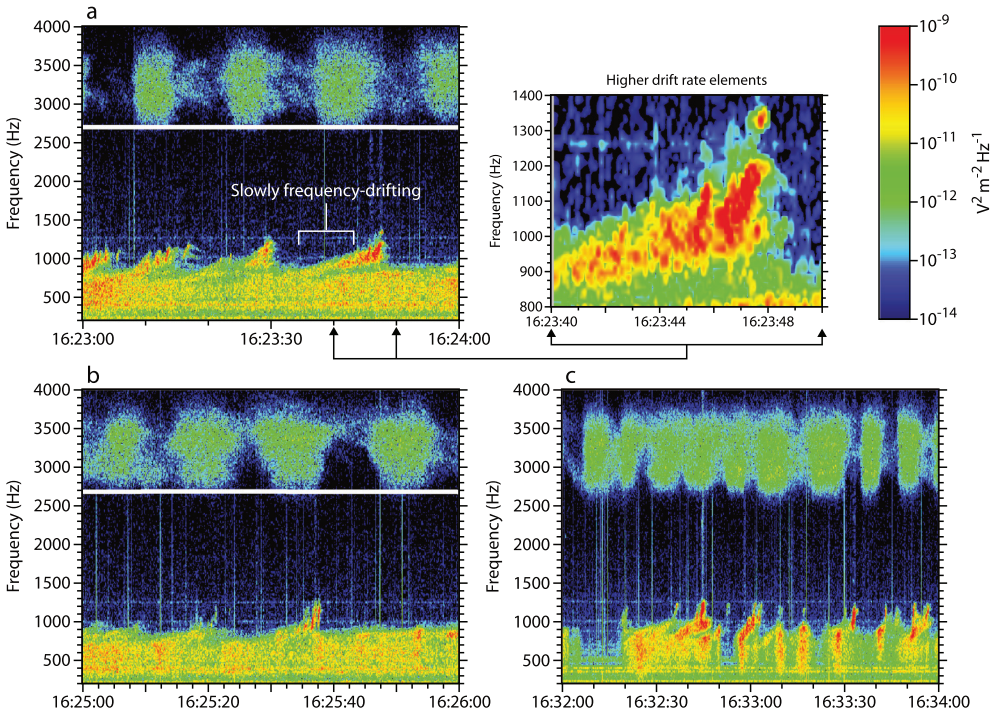

Figure 9. A higher-resolution version of Figure 8 where it appears the chorus emission and ECH emission may be correlated. The slowly drifting-frequency chorus emissions often seem to be distinct from lower frequency emissions. (a, b) The drifting frequency chorus emissions are most intense near and within the period of time when the ECH emissions are most intense. (c) A 2 min interval a little later in time, the drifting frequency chorus emissions vary in phase relative to the ECH emission.

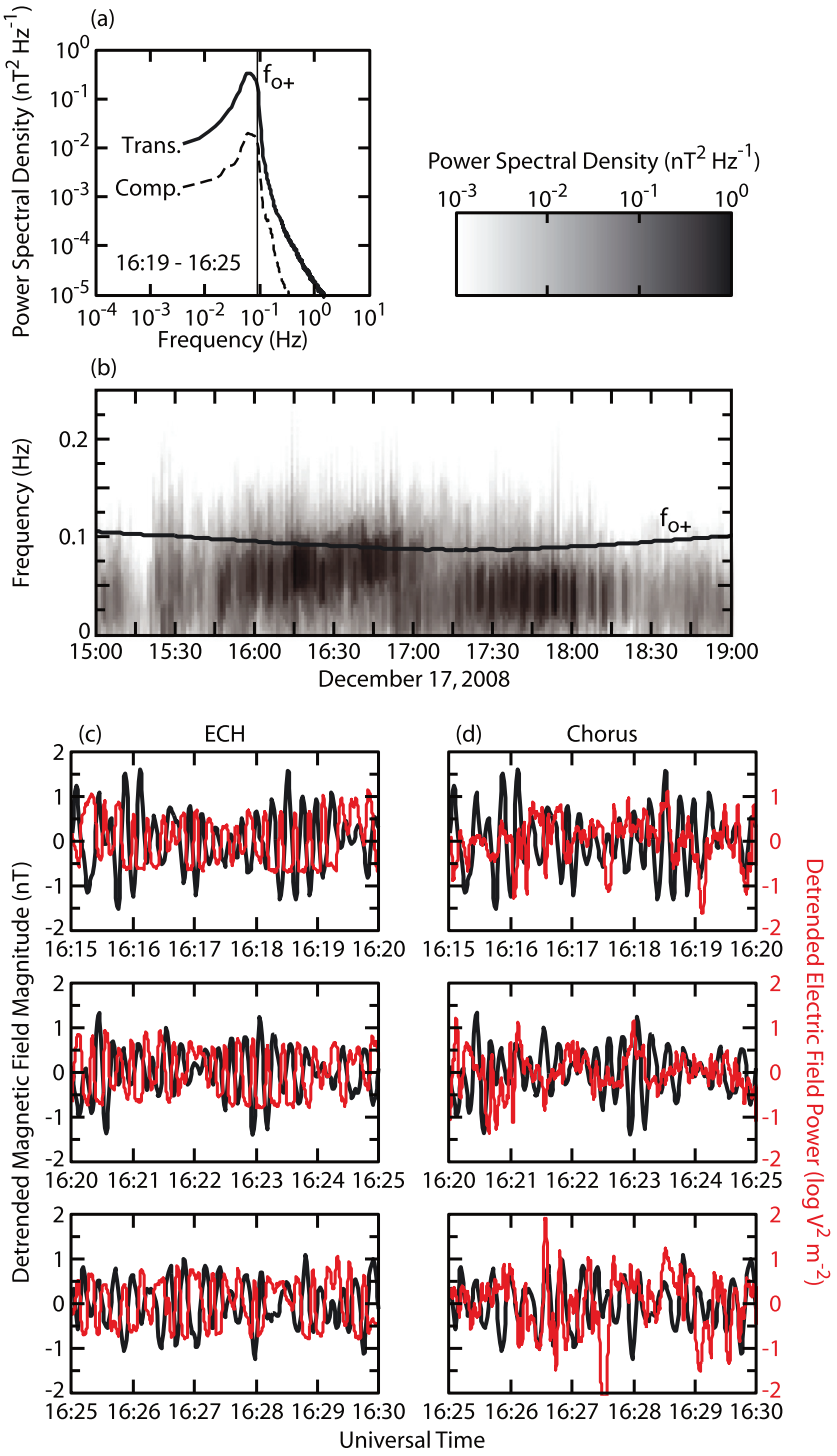

Figure 10. Ion cyclotron wave observations on 17 December 2008. (a) Average power spectrum between 16:19 and 16:25. The dark line labeled "Trans." is the transverse wave power (perpendicular to the magnetic field). The lighter line labeled "Comp." is the compressional wave power (along the magnetic field). The vertical line near 0.1 Hz is the O^+ gyrofrequency during this period of time. (b) Spectrogram of the total ion cyclotron wave power during this equatorial crossing (~17:10). The black line marks the O^+ gyrofrequency across the interval. The differences between the peak wave frequency and the gyrofrequency in the two hemispheres is due to Doppler shift [*Leisner et al.*, 2011]. (c) Magnetic field oscillations (black) obtained by the magnetometer on board Cassini during a time that overlaps the RPWS wideband data. Although not constant, the period of the EMIC waves is frequently the same as the ECH emissions. The envelope of higher-frequency ECH wave power (arbitrary units) is overplotted in red showing the modulation due to the EMIC waves. (d) Chorus power (arbitrary units) integrated over the frequency range 500Hz $<$ f $<$ 1500 Hz is overplotted in red on the EMIC wave oscillations.

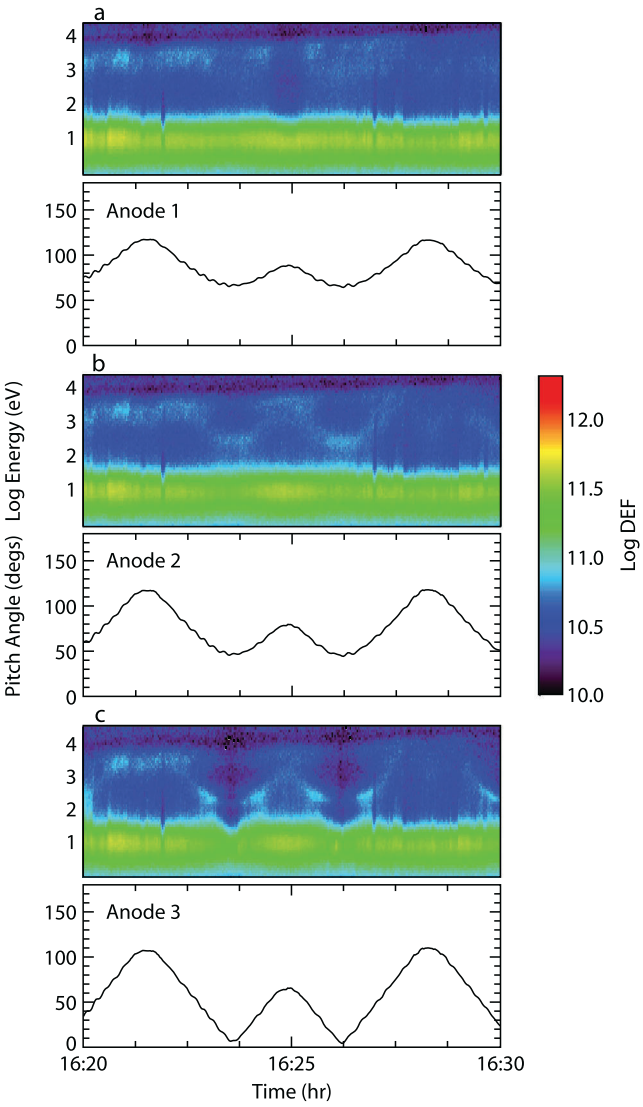

Figure 11. (a, b, c) Differential energy flux (DEF) is plotted for three of the eight fan-arranged anodes of the Cassini ELS instrument, with the bottom panel of each figure showing the pitch angle range for each anode as a function of time. The pitch angle range is increasingly closer to field-aligned proceeding from Figures 11a to 11c. Particularly in Figure 11c, two distinct electron populations for E > 100eV are seen: a higher energy nearly isotropic distribution and a lower energy population which shows a dependence on pitch angle, with lowest energies at the smallest pitch angles.

with lowest energies at the smallest pitch angles. This is similar to electron and ion velocity-filtered distributions reported by *Burch et al.* [1982] for injected plasma in the terrestrial cusp region. The higher energy electron population is the source of the lower frequency hiss-like whistler mode emissions as discussed above. It contains a temperature anisotropy that is unstable to linear growth as previously shown. The lower energy electron population may be the source of the higher frequency chorus seen in Figures 8 and 9 that appears to be distinct from the lower frequency whistler mode emission, sometimes showing a small gap in emission between the two components. While these two electron populations are seen clearly in plots of the DEF, they are not clearly discerned in the contour plots of the PSD (Figure 4). The growth calculations depend on the gradients of the electron PSD.

[15] As discussed by *Gurnett and Bhattacharjee* [2005], the whistler mode resonance energy for an electron plasma is given by

$$W_{\parallel res} = W_c\left(1-\frac{\omega}{\Omega_c}\right)^3\left(\frac{\Omega_c}{\omega}\right), \tag{1}$$

where

$$W_c = \frac{B^2}{(2\mu_0 n_0)}, \tag{2}$$

with ω and Ω_c the wave and cyclotron frequency, respectively, B is the ambient magnetic field intensity, and μ_o the permeability, n_o is the electron number density. For $f_c = 2692$ Hz and $f_p = 42.5$ kHz, we find $W_{\parallel res} \sim 400$eV for f = 1.2kHz and $W_{\parallel res} \sim 3$keV for f = 500Hz. It is possible that the observed chorus at f > 600 Hz, slowly drifting in frequency (~10–20 Hz/s), may have the lower energy electrons (Figure 11c) as a free-energy source.

[16] The slow frequency drift rate of this separate higher frequency component of chorus may be related to the hypothesized modulating energy density of the source electron population due to the stimulating EMIC wave period (~ 14 s.). Oscillations of electron energy density with a period of ~ 14 s would not be observable by CAPS/ELS due to the lack of sampling time at each pitch angle. It is conceivable that oscillating electric field energy density of the EMIC waves modulates the thermal energy of the electrons, which in turn then resonate with whistler mode chorus. These hypotheses should be investigated in future modeling studies.

2.3. Wave Threshold and Optimum Intensity

[17] *Omura et al.* [2009] and *Omura and Nunn* [2011] have presented theory for the nonlinear generation of chorus

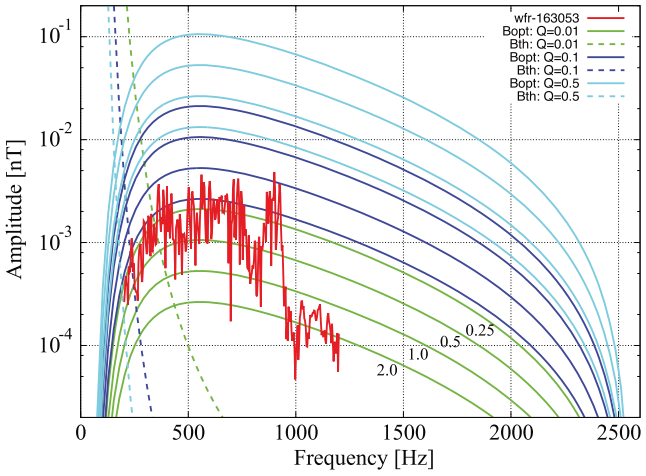

Figure 12. Frequency profiles of the wave amplitudes of the chorus elements. Colored dashed and dotted lines show the optimum (opt) and threshold (th) nonlinear wave amplitudes for the listed values of Q and τ. The plots include observed wave amplitudes (red) near 16:23.

Table 3. Parameters for Wave Amplitude Calculations

Time	f_c(Hz)	$V_{t\|\|}$ (m/s)	$T_\perp/T_\|\|$	N_c (m^{-3})	N_h(m^{-3})
16:23:13	2692.	1.86×10^7	1.42	2.23×10^7	5.15×10^4

elements that describe the threshold wave amplitude and optimum amplitude of nonlinear waves propagating away from the equator source region. *Kurita et al*. [2012] have used this theory to favorably compare the nonlinear wave threshold and optimum amplitude of terrestrial chorus observations obtained by THEMIS satellites. Equations (27) and (25) of *Omura and Nunn* [2011] express the threshold wave amplitude and optimum wave amplitude, respectively, as

$$\widetilde{\Omega}_{th} = \frac{100\pi^3\gamma^3\xi}{\widetilde{\omega}\widetilde{\omega}_{ph}^4\widetilde{V}_{\perp0}^5\delta^5}\left(\frac{\widetilde{a}s_2\widetilde{U}_{t\|}}{Q}\right)^2\exp\left(\frac{\gamma^2\widetilde{V}_R^2}{\widetilde{U}_{t\|}^2}\right), \quad (3)$$

$$\widetilde{\Omega}_{wo} = 0.81\pi^{-5/2}\frac{Q}{\tau}\frac{s_1\widetilde{V}_g}{s_0\widetilde{\omega}\widetilde{U}_{t\|}}\left(\frac{\widetilde{\omega}_{ph}\widetilde{V}_{\perp0}\delta}{\gamma}\right)^2\exp\left(-\frac{\gamma^2\widetilde{V}_R^2}{2\widetilde{U}_{t\|}^2}\right). \quad (4)$$

[18] Details are given in the above articles, but we briefly identify the parameters. Q is the depth of the electromagnetic electron hole in velocity phase space. A value of $Q=1$ means the electron hole is devoid of electrons (strong trapping potential). Other parameters include $\gamma = \left[1-(v/c)^2\right]^{-1/2}$, $\xi^2 = \omega(\Omega_e-\omega)/\omega_p^2$, with $\omega = 2\pi f$, $\omega_p = 2\pi f_p$, $\delta^2 = (1+\xi^2)^{-1}$, τ is the ratio of T_N to the nonlinear trapping period $T_{tr} = 2\pi/\omega_{tr}$, ω_{tr} is the trapping frequency [*Omura et al*., 2008], $s_0 = V_{\perp0}\delta/\xi c$, $s_1 = \gamma\left(1-V_R/V_g\right)^2$, $\widetilde{V}_g = V_g/c$, $\widetilde{\omega} = \omega/\Omega_e$, $\widetilde{U}_{t\|} = U_{t\|}/c = \gamma V_{t\|}/c$, $\widetilde{\omega}_{ph} = \omega_{ph}/\Omega_e$, $\omega_{ph} = \omega_{pe}(N_h/N_c)^{1/2}$, $\widetilde{V}_{\perp0} = V_{\perp0}/c$, $\widetilde{V}_R = V_R/c$, and $V_R = \frac{1}{k}(\omega-\Omega_e/\gamma)$. $V_{t\|}, N_h$, and N_c are thermal velocity of energetic electrons parallel to the ambient magnetic field, and the number density of hot electrons and the number density of cold electrons, respectively. *Omura and Nunn* [2011] define T_N as the nonlinear transition time for formation of the nonlinear resonant current. $V_{\perp0}$ is obtained from the fitting parameters of Table 1, $V_{\perp0} = V_{t\|}\sqrt{T_\perp/T_\|}$. The s_2 is defined in *Omura and Nunn* [2011] in terms of the above parameters.

[19] We have calculated these nonlinear wave amplitudes for the case of chorus emission near 16:23 (Figure 12) during the period of strong nonlinear chorus emission. Parameters for equations 3 and 4 are presented in Table 3 (derived from Table 1, except f_c). The format of Figure 12 is similar to that presented by *Kurita et al*. [2012] for THEMIS results at Earth. As a function of frequency, for each value of Q, the threshold nonlinear wave amplitude is plotted and four corresponding curves of optimum amplitude corresponding to $\tau = 0.25, 0.5, 1., 2$. Superposed on Figure 12 are the observed wave magnetic amplitudes in red. We have used three-axis magnetic search coil data obtained from the RPWS Waveform receiver (WFR) for the wave amplitude. For Figure 12, the closest available snapshot was 16:30:53. A reasonable agreement of the observed chorus threshold and optimum frequency occurs for $Q > 0.1$. *Kurita et al*. [2012] found a good agreement for terrestrial nonlinear chorus for $Q = 0.5$. This smaller value of Q could be related to the large spatial scale of Saturn's magnetosphere. The observed rising chorus tones indicate chorus generated by nonlinear resonant currents, which are created through the formation process of an electromagnetic electron hole in the wave phase space. The intensity of resonant currents is related to the depth of the hole, represented by Q. While strong resonant currents would be required in a relatively smaller system (such as the Earth's magnetosphere) with a large magnetic field inhomogeneity (or gradient), the small inhomogeneity of Saturn's magnetosphere makes it possible for nonlinear effects to emerge for smaller Q. Recently, *Katoh and Omura* [2013] have studied the effects of background magnetic field inhomogeneities on the generation processes of whistler mode chorus and broadband hiss-like emissions at Earth. They have shown that a small spatial inhomogeneity allows the triggering process of rising tone elements to emerge easily.

[20] In Figure 13. we show a high-resolution plot of the chorus waveform of B_y at 16:30:53, the time of data shown in Figure 12. We find strong amplitude modulation of the chorus waveform, which is similar to subpacket structures of chorus elements [*Santolik et al*., 2003]. These subpacket structures are the signature of a series of nonlinear triggering processes to form a rising tone chorus element [e.g., *Katoh and Omura*, 2013]. Figure 13 is evidence that the wave element is generated by a nonlinear triggering process occurring in the Saturn magnetosphere.

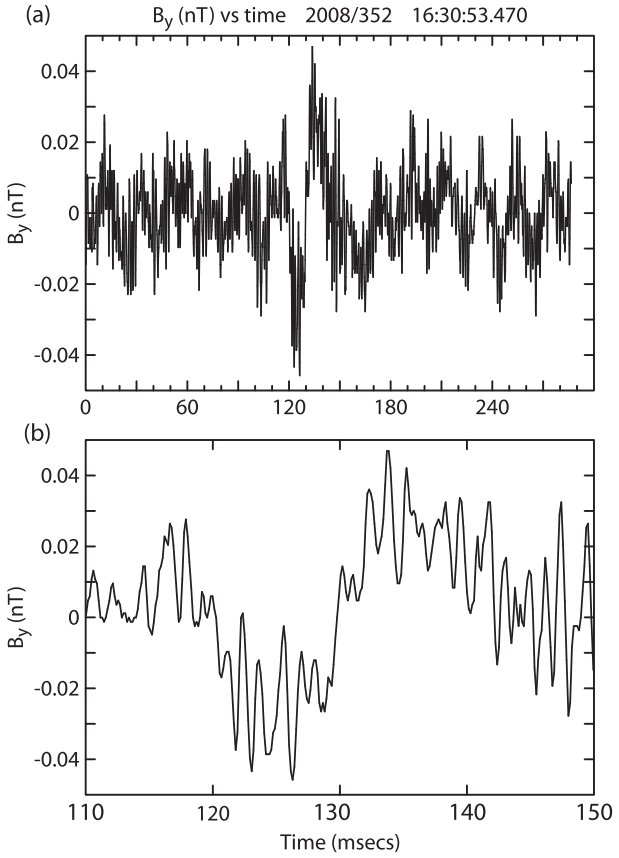

Figure 13. (a) The 287 ms snapshot of B_y amplitude obtained at 16:30:53 by the RPWS WFR. (b) A higher-resolution plot of this data clearly showing the nonconstant nature of the amplitude.

3. Summary and Conclusions

[21] We have presented examples of whistler mode and chorus plasma wave emissions observed at Saturn near the magnetic equator. During crossings of the magnetic equator along nearly constant L shells, the Cassini RPWS observes a local decrease in whistler mode intensity and bandwidth closest to the magnetic equator, where linear growth appears to dominate, with nonlinear, frequency-drifting structures appearing at higher latitudes and higher frequencies.

[22] Using the WHAMP dispersion solver and locally observed electron phase space density measurements from the Cassini Electron Spectrometer (CAPS/ELS), we determine the parameters responsible for the variation in chorus intensity and bandwidth. We find that a temperature anisotropy ($T_\perp/T_\parallel \sim 1.3$) can account for linear spatiotemporal growth rate of the whistler mode emission, which provides a majority of the observed frequency-integrated power. At the highest frequencies, intense, nonlinear, frequency-drifting structures are observed a few degrees away from the equator, and, at times, account for half of the total chorus power. Linear growth of whistler mode waves dominates near the magnetic equator. The linear spatial growth of this emission measured near the equator can easily account for the observed wave power as a function of latitude. Most of the frequency-integrated wave power is provided by the lower frequency emissions, but the nonlinear chorus emissions, when present, can be dominant.

[23] Electromagnetic ion cyclotron waves are frequently observed near the magnetic equator in the inner Saturn magnetosphere [*Leisner et al*., 2006; *Russell et al*., 2006]. Observed moderate amplitude (~ 2nT) EMIC waves modulate the power of the observed ECH emissions with a somewhat irregular period of ~10 to 15 s. Chorus emission appears to be loosely correlated with ECH emissions that are observed, but shifting in phase, perhaps due to the different source locations of each wave.

[24] Chorus emission at higher frequencies ($f \gtrsim 600$ Hz) is sometimes distinct from lower frequency whistler mode emission. This distinct frequency range of chorus may have a source in a lower energy electron component apparent in plots of the electron differential energy flux but not visible in contours of the phase space density. This chorus displays a slow frequency drift (10 to 15 Hz/s) and then develops a fine structure of nonlinear growth with larger frequency sweep rate (~ 200 Hz/s) that can be explained by the theory of *Omura et al*. [2008] [cf. *Menietti et al*., 2013]. This cycle of slow frequency drift developing into nonlinear growth lasts for a period similar to that of the EMIC waves. We hypothesize the EMIC waves may modulate the electron energy density which in turn modifies the growth of the chorus emissions. *Beesho and Menietti* [2007] used simulations to demonstrate how EMIC waves modulate the growth of terrestrial auroral kilometric radiation. *Li et al*. [2011] have shown how compressional PC4–5 waves can modulate the growth of chorus by modulating the density in the source region. Further comprehensive investigation and modeling of the interaction of EMIC waves with chorus and ECH waves at Saturn remain to be done.

[25] Calculations of threshold and optimum amplitudes show reasonable agreement to nonlinear theory for drifting frequency chorus observed for moderately low values of parameter Q, the depth of the electron hole potential. The recent work of *Katoh and Omura* [2013] suggests that the nonlinear triggering process of rising tone elements emerges easily in a smaller background magnetic field inhomogeneity. Since the depth of the hole is related to the intensity of the nonlinear interaction process, the smaller value of Q may be explained by the larger scale sizes at Saturn. More definitive statements await further investigations of the influence of Saturn background magnetic field inhomogeneities, EMIC waves, modulating chorus wave amplitude, and perhaps even higher-resolution wave observations.

[26] **Acknowledgments.** We wish to thank J. Barnholdt for administrative assistance and J. Chrisinger for help with several plots. J.D.M. acknowledges support from JPL contract 1415150 and NASA grant NNX11AM36G. The work of Y.K. was partially supported by grant-in-aid 23224011 of the Ministry of Education, Culture, Sports, Science, and Technology in Japan. O.S. acknowledges support from grants GACR205-10/2279 and LH12231.

[27] Masaki Fujimoto thanks the reviewers for their assistance in evaluating this paper.

References

Beesho, N., J. D. Menietti (2007), Particle-in-cell simulation study of the impact of ion cyclotron waves on auroral kilometric radiation, *J. Geophys. Res.*, *112*, A10215, doi:10.1029/2007JA012417.

Bortnik, J., R. M. Thorne, and U. S. Inan (2008), Nonlinear interaction of energetic electrons with large amplitude chorus, *Geophys. Res. Lett.*, *35*, L21102, doi:10.1029/2008GA035500.

Burch, J. L., P. H. Reiff, R. A. Heelis, J. D. Winningham, W. B. Hanson, C. Gurgiolo, J. D. Menietti, R. A. Hoffman, and J. N. Barfield (1982), Plasma injection and transport in the mid-altitude polar cusp, *Geophy. Res. Lett.*, *9*(9), 921–924, doi:10.1029/GL009i009p00921.

Carlson, C. W., et al. (1998), FAST observations in the downward auroral current region: Energetic upgoing electron beams, parallel potential drops, and ion heating, *Geophys. Res. Lett.*, *25*(12), 2017–2020, doi:10.1029/98GL00851.

Chaston, C. C., J. W. Bonnell, J. P. McFadden, R. E. Ergun, and C. W. Carlson (2002), Electromagnetic ion cyclotron waves at proton cyclotron harmonics, *J. Geophys. Lett*, *107*(A11), 1351, doi:10.1029/2001JA900141.

Dougherty, M. K., et al. (2005), Cassini magnetometer observations during Saturn orbit insertion, *Science*, *307*, 1266–1270, doi:10.1126/science.1106098.

Gurnett, D. A., and A. Bhattacharjee (2005), *Introduction to Plasma Physics*, p. 379, Cambridge Univ. Press, Cambridge, U. K.

Gurnett, D. A., et al. (2004), The Cassini radio and plasma wave investigation, *Space Sci. Rev.*, *114*(1–4), 395–463, doi:10.1007/s11214-004-1434-0.

Haque, N., U. S. Inan, T. F. Bell, and J. S. Pickett (2012), Spatial dependence of banded chorus intensity near the magnetic equator, *Geophys. Res. Lett.*, *39*, L17103, doi:10.1029/2012GL052929.

Horne, R. B., and R. M. Thorne (2000), Electron pitch angle diffusion by electrostatic electron cyclotron harmonic waves: The origin of pancake distributions, *J. Geophys. Res.*, *105*(A3), 5391–5402, doi:10.1029/1999JA900447.

Horne, R. B., R. M. Thorne, S. A. Glauert, D. J. Menietti, Y. Y. Shprits, and D. A. Gurnett (2008), Gyro-resonant electron acceleration at Jupiter, *Nature Physics*, *4*, 301–304, doi:10.1038/nphys897.

Hospodarsky, G. B., K. Sigsbee, J. S. Leisner, J. D. Menietti, W. S. Kurth, D. A. Gurnett, C. A. Kletzing, and O. Santolik (2012), Plasma wave observations at Earth, Jupiter, and Saturn, in *Dynamics of the Earth's Radiation Belts and Inner Magnetosphere*, Geophys. Monogr. Ser., vol. 199, edited by D. Summers et al., pp. 415–430, AGU, Washington, D. C.

Katoh, Y., and Y. Omura (2004), Acceleration of relativistic electrons due to resonant scattering by whistler mode waves generated by temperature anisotropy in the inner magnetosphere, *J. Geophys. Res.*, *109*, A12214, doi:10.1029/2004JA010654.

Katoh, Y., and Y. Omura (2006a), Simulation study on nonlinear frequency shift of narrow band whistler-mode waves in a homogeneous magnetic field, *Earth Planets Space*, *58*(9), 1219–1225.

Katoh, Y., and Y. Omura (2006b), A study of generation mechanism of VLF triggered emission by self-consistent particle code, *J. Geophys. Res.*, *111*, A12207, doi:10.1029/2006JA011704.

Katoh, Y., and Y. Omura (2007a), Computer simulation of chorus wave generation in the Earth's inner magnetosphere, *Geophys. Res. Lett.*, *34*, L03102, doi:10.1029/2006GL028594.

Katoh, Y., and Y. Omura (2007b), Relativistic particle acceleration in the process of whistler-mode chorus wave generation, *Geophys. Res. Lett.*, *34*, L13102, doi:10.1029/2007GL029758.

Katoh, Y., and Y. Omura (2011), Amplitude dependence of frequency sweep rates of whistler mode chorus emissions, *J. Geophys. Res.*, *116*, A07201, doi:10.1029/2011JA016496.

Katoh, Y., and Y. Omura (2013), Effect of the background magnetic field inhomogeneity on generation processes of whistler-mode chorus and broadband hiss-like emissions, *J. Geophys. Res. Space Physics*, *118*, 4189–4198, doi:10.1002/jgra.50395.

Kurita, S., Y. Katoh, Y. Omura, V. Angelopoulos, C. M. Cully, O. Le Contel, and H. Misawa (2012), THEMIS observations of chorus elements without a gap at half the gyrofrequency, *J. Geophys. Res.*, *117*, A11223, doi:10.1029/2012JA018076.

Leisner, J. S., C. T. Russell, M. K. Dougherty, X. Blanco-Cano, R. J. Strangeway, and C. Bertucci (2006), Ion cyclotron waves in Saturn's E ring: Initial Cassini observations, *Geophys. Res. Lett.*, *33*, L11101, doi:10.1029/2005GL024875.

Leisner, J. S., C. T. Russell, H. Y. Wei, and M. K. Dougherty (2011), Probing Saturn's ion cyclotron waves on high-inclination orbits: Lessons for wave generation, *J. Geophys. Res.*, *116*, A09235, doi:10.1029/2011JA016555.

Li, W., R. M. Thorne, J. Bortnik, Y. Nishimura, and V. Angelopoulos (2011), Modulation of whistler mode chorus waves: 1. Role of compressional Pc4–5 pulsations, *J. Geophys. Res.*, *116*, A06205, doi:10.1029/2010JA016312.

Lysak, R., M. Hudson, and M. Temerin (1980), Ion heating by strong electrostatic ion cyclotron turbulence, *J. Geophys. Res.*, *85*(A2), 678–686, doi:10.1029/JA085iA02p00678.

Mauk, B. H., and N. J. Fox (2010), Electron radiation belts of the solar system, *J. Geophys. Res.*, *115*, A12220, doi:10.1029/2010JA015660.

Menietti, J. D., P. Schippers, O. Santolik, D. A. Gurnett, F. Crary, and A. J. Coates (2011), Ion cyclotron harmonics in the Saturn downward current auroral region, *J. Geophys. Res.*, *116*, A12234, doi:10.1029/2011JA017102.

Menietti, J. D., Y. Y. Shprits, R. B. Horne, E. E. Woodfield, G. B. Hospodarsky, and D. A. Gurnett (2012), Chorus, ECH, and Z mode emissions observed at Jupiter and Saturn and possible electron acceleration, *J. Geophys. Res.*, *117*, A12214, doi:10.1029/2012JA018187.

Menietti, J. D., Y. Katoh, G. B. Hospodarsky, and D. A. Gurnett (2013), Frequency drift of Saturn chorus emission compared to nonlinear theory, *J. Geophys. Res. Space Physics*, *118*, 982–990, doi:10.1002/jgra.50165.

Nunn, D., Y. Omura, H. Matsumoto, I. Nagano, and S. Yagitani (1997), The numerical simulation of VLF chorus and discrete emissions observed on the Geotail satellite using a Vlasov code, *J. Geophys. Res.*, *102*(A12), 27,083–27,097, doi:10.1029/97JA02518.

Omura, Y., and D. Nunn (2011), Triggering process of whistler-mode chorus emissions in the magnetosphere, *J. Geophys. Res.*, *116*, A05205, doi:10.1029/2010JA016280.

Omura, Y., and D. Summers (2004), Computer simulations relativistic whistler-mode wave-particle interactions in the magnetosphere, *Phys. Plasmas*, *11*, 3530–3534, doi:10.1063/1.1757457.

Omura, Y., and D. Summers (2006), Dynamics of high-energy electrons interacting with whistler mode chorus emissions in the magnetosphere, *J. Geophys. Res.*, *111*, A09222, doi:10.1029/2006JA011600.

Omura, Y., N. Furuya, and D. Summers (2007), Relativistic turning acceleration of resonant electrons by coherent whistler mode waves in a dipole magnetic field, *J. Geophys. Res.*, *112*, A06236, doi:10.1029/2006JA012243.

Omura, Y., Y. Kato, and D. Summers (2008), Theory and simulation of the generation of whistler-mode chorus, *J. Geophys. Res.*, *113*, A04223, doi:10.1029/2007JA012622.

Omura, Y., M. Hikishima, Y. Katoh, D. Summers, and S. Yagitani (2009), Nonlinear mechanisms of lower-band and upper-band VLF chorus emissions in the magnetosphere, *J. Geophys. Res.*, *114*, A07217, doi:10.1029/2009JA014206.

Rönnmark, K. (1982), WHAMP – waves in a homogeneous anisotropic multicomponent plasma, *Rep. 179*, Kiruna Geophys. Inst., Kiruna, Sweden.

Rönnmark, K. (1983), Computation of the dielectric tensor of a Maxwellian plasma, *Plasma Phys.*, *25*(6), 699–701, doi:10.1088/0032-1028/25/6/007.

Russell, C. T., J. S. Leisner, C. S. Arridge, M. K. Dougherty, and X. Blanco-Cano (2006), Nature of magnetic fluctuations in Saturn's middle magnetosphere, *J. Geophys. Res.*, *111*, A12205, doi:10.1029/2006JA011921.

Santolik, O., D. A. Gurnett, J. S. Pickett, M. Parrot, and N. Comilleau-Wehrlin (2003), Spatio-temporal structure of storm-time chorus, *J. Geophys. Res.*, *108*, 1278, doi:10.1029/2002JA009791.

Santolik, O., D. A. Gurnett, J. S. Pickett, J. Chum, and N. Cornilleau-Wehrlin (2009), Oblique propagation of whistler mode waves in the chorus source region, *J. Geophys. Res.*, *114*, A00F03, doi:10.1029/2009JA014586.

Shprits, Y. Y., D. J. Menietti, X. Gu, K. C. Kim, and R. B. Horne (2012), Gyroresonant interactions between the radiation belt electrons and whistler mode chorus waves in the radiation environments of Earth, Jupiter, and Saturn: A comparative study, *J. Geophys. Res.*, *117*, A11216, doi:10.1029/2012JA018031.

Summers, D., and Y. Omura (2007), Ultra-relativistic acceleration of electrons in planetary magnetospheres, *Geophys. Res. Lett.*, *34*, L24205, doi:10.1029/2007GL032226.

Summers, D., Y. Omura, Y. Miyashita, and D.-H. Lee (2012), Nonlinear spatiotemporal evolution of whistler mode chorus waves in Earth's inner magnetosphere, *J. Geophys. Res.*, *117*, A09206, doi:10.1029/2012JA017842.

Trakhtengerts, V. Y. (1999), A generation mechanism for chorus emission, *Ann. Geophys.*, *17*, 95–100, doi:10.1007/s00585-999-0095-4.

Trakhtengerts, V. Y., M. J. Rycroft, and A. G. Demekhov (1996), Interrelation of noise-like and discrete ELF/VLF emissions generated by cyclotron interactions, *J. Geophys. Res.*, *101*(A6), 13,293–13,301, doi:10.1029/95JA03515.

Young, D. T., et al. (2004), Cassini plasma spectrometer investigation, *Space Sci. Rev.*, *114*(1–4), 1–112, doi:10.1007/s11214-004-1406-4.